



**Decorating γ -alumina solid-state electrolyte with
submicron Pb spherical particles to overcome liquid-solid
interface resistance**

Journal:	<i>Journal of Materials Chemistry A</i>
Manuscript ID	TA-ART-07-2018-006745.R1
Article Type:	Paper
Date Submitted by the Author:	29-Aug-2018
Complete List of Authors:	<p>Chang, Hee-Jung; Pacific Northwest National Laboratory, Energy Materials Lu, Xiaochuan; Pacific Northwest National Laboratory, Energy & Environment Division Bonnett, Jeff; Pacific Northwest National laboratory, Energy and Environment Directorate Canfield, Nathan; Pacific Northwest National Laboratory, Energy Materials Han, Kee Sung; Pacific Northwest National Laboratory, Environmental Molecular Science laboratory Engelhard, Mark; Pacific Northwest National laboratory, Environmental Molecular Sciences Laboratory Jung, Keeyoung; Research Institute of Industrial Science and Technology, Energy Storage Materials Research Group Sprenkle, Vincent; Pacific Northwest National Laboratory, Li, Guosheng; Pacific Northwest National Laboratory, Energy Materials</p>



Journal Name

ARTICLE

Decorating β'' -alumina solid-state electrolyte with submicron Pb spherical particles for improving Na wettability at lower temperatures

Received 00th January 20xx,
Accepted 00th January 20xx

DOI: 10.1039/x0xx00000x

www.rsc.org/

Hee Jung Chang,^a Xiaochuan Lu,^a Jeffery F. Bonnett,^a Nathan L. Canfield,^a Keesung Han,^b Mark H. Engelhard,^c Keeyoung Jung,^{d,*} Vincent L. Sprenkle,^a and Guosheng Li^{a,*}

Overcoming the poor physical contact is one of the most critical hurdles for batteries using solid-state electrolytes. In particular, overpotential from the liquid-solid interface between molten sodium and β'' -alumina solid-state electrolyte (BASE) in a sodium-metal halide (Na-MH) battery could be enormous at lower operating temperatures (<200°C) due to intrinsically poor Na wetting on the BASE surface. In this work, we describe how surface modification by lead acetate trihydrate (LAT) at different temperatures affects Na wetting on the BASEs. LAT treatment conducted at a temperature of 400°C (under nitrogen gas atmosphere) shows significantly better Na wettability and battery performance than treatments at lower temperatures. The formation of a unique morphology—submicron-size Pb spherical particles—is observed on the surface of BASE LAT treated at 400°C. We also observed an evolution of the Na wetting configuration from Cassie drop, to Wenzel drop, and finally to sunny-side-up drop, which are clearly different from Young-Dupré relation, as increasing the contact-angle measurement temperature. We conclude that formation of a thin Na penetrating film (sunny-side-up shape) on Pb-decorated BASEs is crucial for achieving good battery performance at lower operating temperatures. The new observations and fundamental understanding of Na wetting reported here will provide excellent guidance for improving cell performance in general, and will further promote development of practical Na-MH battery technologies for large-scale energy storage applications.

Introduction

With the rapid deployment of renewable energy resources, such as wind power and photovoltaic cells, the traditional electrical power grid faces tremendous opportunities and challenges toward maintaining grid reliability, sustainability, resiliency, and efficient electricity utilization. In this regard, stationary energy storage systems have become one of the most important components for the next-generation (smart) grid, since they can effectively integrate intermittent renewables and provide viable grid services such as frequency regulation, arbitrage, peak shaving, and microgrids.¹ Therefore, increasing attention has been given to developing feasible battery technologies for stationary storage applications, which require superior safety and reliability, longer cycle life, and

substantially lower cost.²⁻³ The use of a naturally abundant element—sodium (Na)—as the charge carrier rather than lithium (Li) is an attractive way to reduce materials cost.⁴⁻⁵ Among various Na based battery technologies, Na β'' -alumina batteries (NBBs) including Na-S and Na-metal halide batteries (Na-MH or Zebra), have been extensively investigated and demonstrated due to their potentially low cost, since both batteries employ readily available/abundant elements e.g. Na, S, Fe, Ni, O, and Cl.⁶⁻⁷ However, the high operating temperature of conventional NBBs (350°C for Na-S and 280°C for Na-NiCl₂ batteries) significantly raises the cost of batteries due to intrinsic issues (complicated cell assembly process, high capital cost, and low production capability), and limits its practical applications as a stationary energy storage device. More recently, planar type NBBs have attracted interest due to advantages such as high power density, simple cell architectures, improved thermal management, lower operating

^a Electrochemical Materials and Systems Group, Pacific Northwest National Laboratory, 902 Battelle Blvd., Richland, WA, USA

^b Materials Science Group, Pacific Northwest National Laboratory, 902 Battelle Blvd., Richland, WA, USA

^c Interfacial Sci's & Simulation Group, Pacific Northwest National Laboratory, 902 Battelle Blvd., Richland, WA, USA

^d Materials Research Division, Research Institute of Industrial Science & Technology, Pohang, South Korea

*Email - Guosheng.Li@pnnl.gov

Electronic Supplementary Information (ESI) available: [Pictures of Na sessile drops, additional SEM images, phase diagram and battery performances]. See DOI: 10.1039/x0xx00000x

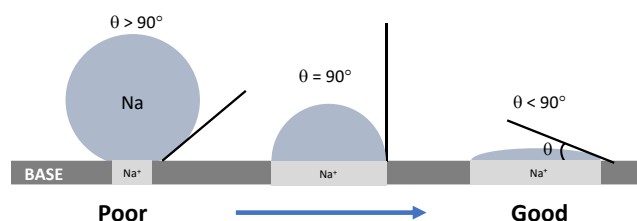


Figure 1. Schematic view of Na droplets on the surface of BASE with different wetting angles (θ).

temperature, and lower manufacturing cost.⁸⁻¹⁰ Material degradation in planar type Na-MH batteries (Ni or NaCl particle growths) is significantly suppressed at lower operating temperatures (<200°C), which allow a prolonged cycle life and stable cell performance.¹¹⁻¹² Moreover, a lower operating temperature enables the use of conventional polymers as sealing materials to replace high-cost sealing technologies (glass seal, thermo-compression bonding, and laser welding) required for the high temperature batteries.¹³

One of main challenges for developing practical lower temperature Na-MH batteries is the unique temperature dependence of the Na wettability on the BASE surface.¹⁴ A few representative interfaces of Na and BASEs are shown in Fig. 1. As one can see, a good sodium wetting (smaller wetting angle, $\theta < 90^\circ$, Fig. 1[right]) on the BASE surface will result in a low overpolarization, which is crucial for Na-MH battery performance. Unfortunately, intrinsic features of molten sodium (the relatively high surface tension of molten sodium (~200 mN/m)¹⁵⁻¹⁶ compared to water (~73 mN/m)¹⁷) and the surface features of BASE (existence of surface adsorbates), tend to work against good Na wetting and lead to poor Na wettability shown on the left side of Fig. 1.¹⁸⁻¹⁹ In the past, various methods have been employed to improve the Na wetting on the BASE surface. For tubular type high temperature Na-S and Zebra batteries, a thin coating of carbon or carbon felt followed by a thermal treatment were applied on the BASE surface to improve the Na anode performance.^{18, 20} It has been also reported that a thin Ni nanofibers coating on the BASE surface improves the Na wettability at near 300°C.²¹ In particular, developing preferable sodium wetting at lower temperatures (<200°C) is crucial for demonstrating lower operating temperature Na-MH batteries. One approach for improving Na wetting on BASE is sputtering a thin layer of metal coatings on vacuum heat-treated BASEs to remove possible impurities on the BASE surface such as moisture and surface hydroxyl groups.²² Another approach is using Na alloys (Na-Cs, Na-Bi), which improve the wettability by larger work of adhesion of Na alloys compared to that of pure Na.^{14, 23} The theoretical root of above approaches is all based on Young-Dupré relation, which represents the wetting phenomenon on an ideal surface (flat and smooth).

In this work, we propose a new mechanism for improving Na wettability through introducing non Young-Dupré relation. Surface treatment using lead acetate trihydrate (LAT)²⁴⁻²⁶ on the BASEs is adopted as a model system to investigate how strategically designed surface morphologies affect the Na wettability. LAT treatment conducted at a temperature of 400°C (under nitrogen gas atmosphere) shows significantly better Na wettability and battery performance than at other temperatures. The formation of a unique morphology—micron-size Pb spherical particles—is observed on the BASE surface LAT treated at 400°C, and this is quite unlike the thin Pb film formation generally presumed in the past. We also found out that the Na wetting phenomena on LAT-treated BASEs can no longer be treated as wetting on an ideal flat surface (Young-Dupré equation). The parameters of surface texture (roughness), which are included in more complicated wetting models such as Cassie, Wenzel, and sunny-side-up drops, should be considered to explain the improved Na wetting phenomena. The fundamental understanding of the Na wetting reported in this work will provide excellent guidance for resolving the liquid-solid contact in Na-MH batteries at lower operating

temperatures, and will further promote the development of practical Na-MH battery technologies for large-scale energy storage applications.

Results

To characterize the decomposition products of LAT, TGA and DTA were conducted with a heating rate of 10°C/min up to 500°C in a dry N₂ atmosphere. Fig. 2a shows TGA and DTA curves of LAT, and five noticeable endothermic processes were detected, which is in good agreement with a previous report.²⁸ The first step appears between 30°C and 100°C with a weight loss of 6% from the initial weight of the lead acetate sample. The decrease in weight started at the beginning of the measurement, and the first two peaks at 66.6°C and 86.3°C are associated with the dehydration process. The second step, which is attributed to the melting of anhydrous lead acetate, occurs at 209.6°C and a slight decrease in weight of 4% was observed. The next two steps appear around 276.4°C and 312.9°C with weight losses of approximately 13% and 5%, respectively. The final step appears in the temperature range 370°C to 400°C with a 14% decrease in weight. The total weight

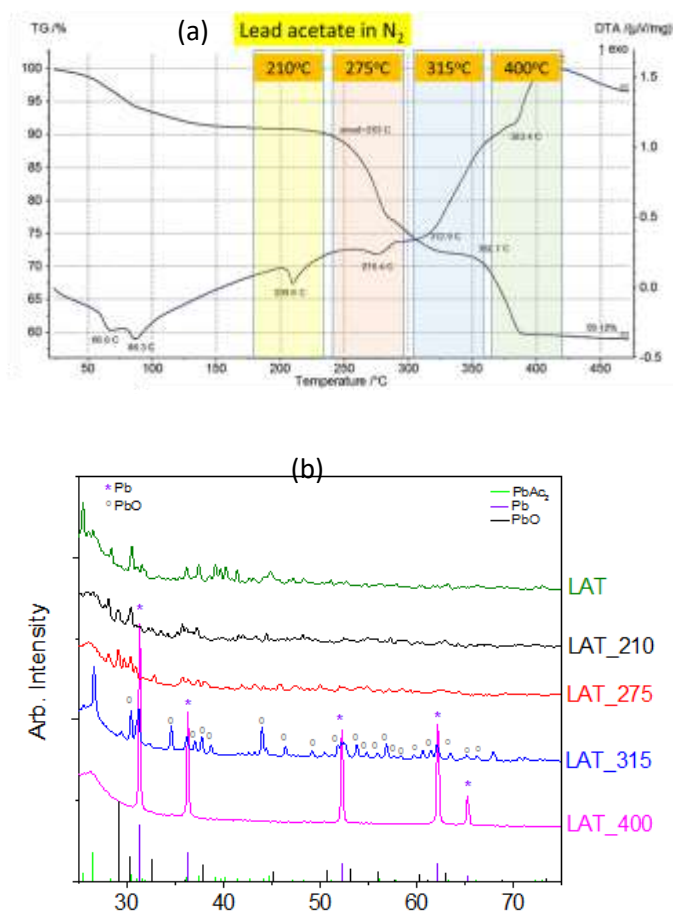


Figure 2. (a) TGA/DTA curves for the decomposition of $\text{Pb}(\text{CH}_3\text{COO})_2 \cdot 3\text{H}_2\text{O}$ (LAT). The experiment was performed under N₂ atmosphere with a heating rate of 10°C/min. (b) XRD powder diffraction of lead acetate and the decomposition products at different temperatures. The Pb and PbO reference peaks are marked by green stars (*) and gray circles, respectively. Standard peaks (Pb, PbO, and LAT) are also shown as stake graphs at the bottom. All XRD samples were prepared under N₂ atmosphere.

loss after completion of the decomposition process at 400°C is 41% with respect to the original sample weight. By considering the systematic errors from the TGA/DTA measurement, the result suggests the final decomposition product can be lead oxide (PbO) or lead (Pb), or a mixture of PbO and Pb, because the reduction of lead acetate to metallic lead theoretically requires about 45.4% of weight loss. Powder X-ray diffraction (XRD) measurements were employed to further identify the thermal decomposition products of LAT. Fig. 2b exhibits XRD peak patterns of LAT thermal decomposition products under N₂ at 210, 275, 315, and 400°C, respectively. In comparison, the XRD pattern of the pristine sample (LAT) is also shown in Fig. 2b (green curve). The pattern of the sample heated at 210°C suggests the formation of a basic acetate salt, Pb(CH₃COO)₂ (Pb(Ac)₂),²⁹ 275°C to produce the second basic Pb(Ac)₂ and PbO (Fig. 2b, red). For the sample heated at 315°C, the assigned XRD pattern indicate the formation of metallic Pb and PbO (blue curve), which were confirmed by the reference patterns of Pb and PbO marked in Fig. 2b. Upon heating to 400°C, the main decomposition product of LAT is metallic lead, which is clearly observed from its XRD patterns (Fig. 2b, pink). According to the TGA/DTA and XRD results shown above, the thermal decomposition process of LAT on the BASE surface can be summarized with the following scheme:²⁹

In agreement with the TGA/DTA results, the XRD results suggest that three basic decomposition products, namely Pb(Ac)₂, PbO, and Pb, are produced during thermal decomposition of LAT, and the ultimate decomposition product

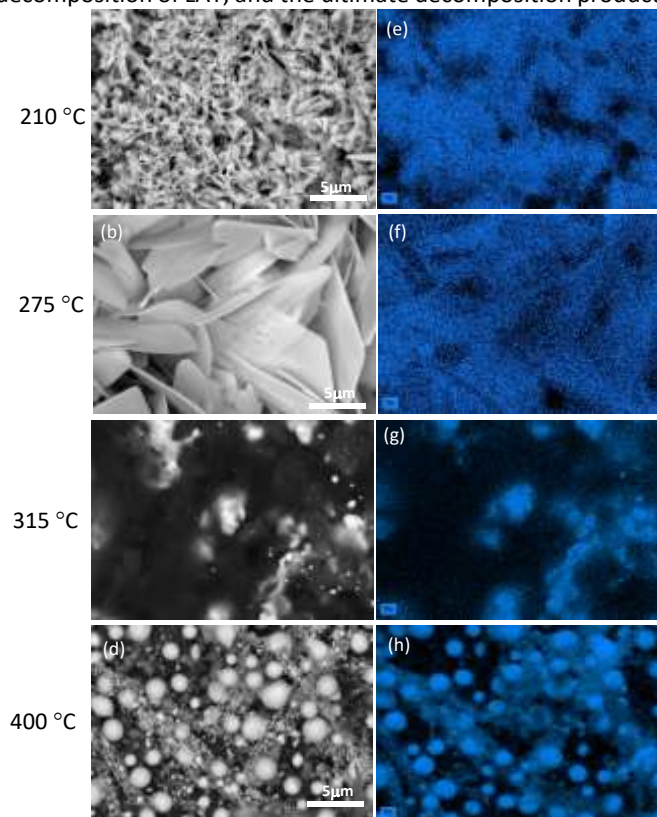


Figure 3. SEM images and EDX maps (Pb) of the decomposition products. (a-d) SEM images of the surface morphology for BASEs LAT treated at 210°C, 275°C, 315°C, and 400°C, respectively. (e-h) Corresponding Pb mapping images for BASEs LAT treated at 210°C, 275°C, 315°C, and 400°C, respectively.

at 400°C is metallic Pb. The proposed thermal decomposition process of LAT shown above is in good agreement with previously reported studies,²⁸⁻²⁹ except forming PbO/Pb at 315°C. Since the temperature range of the formation of metallic Pb is between 312.9 and 383.4°C (shown in Fig. 2a), partial decomposition of Pb(Ac)₂/2PbO at 315°C could result in mixed products of PbO/Pb.

SEM and EDX were carried out to investigate the BASE surface with the LAT heat treatment at different temperatures. As shown in Fig. 3, the decomposition products show drastic changes in morphology with temperatures. Fig. 3a shows that the sample at 210°C (LAT_210°C) has a uniform distribution of sharp, needle-like crystal structures. As the heating temperature increases to 275°C (LAT_275°C), the morphological feature changes to flat, leaf-like structures of larger particle size, >5 μm (Fig. 3b). The corresponding EDX element analysis indicates the compositions are a mixture of C, O, and Pb on both samples (Fig. S1 for 210°C and 275°C). In the decomposition product at 315°C (LAT_315°C), some amorphous features were also observed (Fig. 3c), instead of a certain particle shape or structure seen in the two samples heat treated at lower temperatures. The EDX mapping shows the brighter particle is most likely associated with lead. The most interesting observation is the formation of spherical particles on the BASE surface at 400°C (LAT_400°C), as shown in Fig. 3d. The average particle size is about 1~2 μm and the particles are isolated from each other. The EDX analysis confirms that those are pure metallic lead particles, which is also in good agreement with the XRD pattern of metallic Pb shown in Fig. 2. The darker area appearing as a background is a bare BASE surface, and a small amount of carbon was also detected (Fig. S1). It is not surprising that the trace amount of carbonaceous materials (residues from the thermal decomposition), which was not detected in XRD data, exist most likely in the amorphous phase.

To investigate the wetting behavior of liquid (molten) sodium on BASEs with/without LAT treatment, the sessile drop technique was adopted in this work. A schematic configuration of sessile drops at different contact angles is shown in Fig. 1. By

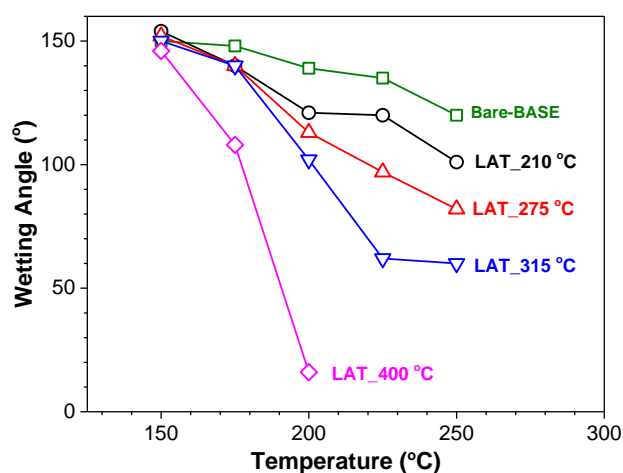


Figure 4. Wetting behavior of Na on BASE surfaces using the sessile drop technique at various temperatures of 150, 175, 200, 225, and 250°C in N₂ atmosphere. Lower wetting angles imply better Na wetting on the BASE.

using the definitions from drop shape analysis, a bead of liquid drop on a solid surface with a contact angle greater than 90° but less than 180° is associated with poor wettability and adhesion (Fig. 1 left). When the contact angle is equal to 90° , it is considered partial wetting (Fig. 1 middle). If the contact angle is less than 90° , the drop spreads over the solid surface, which is defined as high wettability with good adhesion (Fig. 1 right). Fig. 4 compares Na contact angles on a bare BASE and LAT-treated BASEs at measuring temperatures of 150, 175, 200, 225, and 250°C . Detailed pictures of each Na drop for the series of sessile drop experiments can be found in Fig. S2. At 150°C , all of the liquid Na shows poor wettability (high wetting angles, $\sim 150^\circ$) regardless of BASE conditions. It is clear that the wetting angle generally decreases as the measuring temperature increases. However, the progressions of the wetting angles are quite different for BASEs with different LAT treatments. The wettability of Na at 250°C on a bare BASE only improves 20% (120°) compared to the initial angle (150°) measured at 150°C . For LAT_210 $^\circ\text{C}$, LAT_275 $^\circ\text{C}$, and LAT_315 $^\circ\text{C}$, wetting angles at 250°C are 101° , 82° , and 60° , respectively, which are about 34%, 46%, and 60% improvement vs. their initial angles at $\sim 150^\circ\text{C}$,

respectively. Although the wettability of Na gradually increased with temperature, a complete Na wetting was not observed for those BASEs except for the LAT_400 $^\circ\text{C}$. In contrast to the bare and LAT-treated BASEs below 400°C , a significant improvement (89%) was observed only on the LAT_400 $^\circ\text{C}$. The smallest contact angle ($\sim 16^\circ$) was measured at 200°C and indicates almost complete Na wetting on the BASE surface.

To correlate Na wettability with electrochemical performance of batteries, Na-NiCl₂ cells were assembled and tested using the BASE with/without LAT treatment, as shown in Fig. 5. State of charge (SOC) plots at the end of charge (EOC) and the end of discharge (EOD) can be found in Fig. S3. The cell with the bare BASE achieved a charge capacity of $\sim 20\text{mAh}$ ($\sim 13\%$ SOC) during the first cycle and lower charge capabilities for subsequent cycles (Fig. 5a, green). This implies the cathode materials cannot be utilized during charge/discharge processes due to the poor Na wetting on the bare BASE, which is also confirmed from the low EOC shown in Fig. S3(a). In contrast to the bare BASE, the cell using LAT_400 $^\circ\text{C}$ gives a full capacity ($\sim 150\text{mAh}$, $>95\%$ SOC) from the first cycle, and retains its high capacity for subsequent cycles (Fig. 5, pink). The cells having LAT-treated BASEs at lower temperatures show various degrees of degraded performance compared to the LAT_400 $^\circ\text{C}$ cell. For instance, the LAT_210 $^\circ\text{C}$ (Fig. 5a, black) and LAT_275 $^\circ\text{C}$ (red) cells give a significantly lower charge capacity after 10 cycles. Although the LAT_315 $^\circ\text{C}$ cell (Fig. 5a, blue) shows a relatively improved performance comparing to LAT_210 $^\circ\text{C}$ and LAT_275 $^\circ\text{C}$, its charge capacity is still lower than that of the LAT_400 $^\circ\text{C}$ cell by 10 mAh/g. Long-term cycling was performed for the LAT_400 $^\circ\text{C}$ cell with charge and discharge currents of 20 mA and 30 mA, respectively. As shown in Fig. 5b, the LAT_400 $^\circ\text{C}$ cell shows a specific capacity of $\sim 136\text{mAh/g}$ in the beginning and quickly stabilizes at a capacity of $\sim 140\text{mAh/g}$, which is quite consistent with the previously reported results. The coulombic efficiency of LAT_400 $^\circ\text{C}$ is nearly 100% ($\pm 0.05\%$) throughout the long-term cycling test, and it is owing to the use of the Na⁺ ion-conducting BASE, which blocks material crossover except for Na⁺ ions.

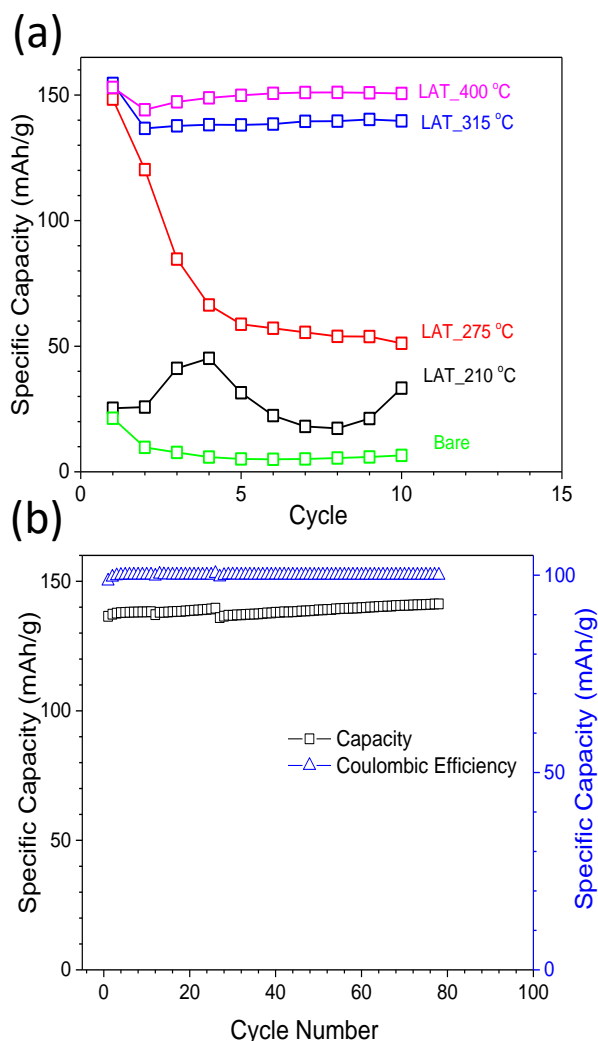


Figure 5. Cell specific capacity of batteries with different LAT-treated BASEs: (a) conditioning cycles (up to 10 cycles), (b) regular cycling for LAT_400 $^\circ\text{C}$ for long-term testing.

Discussion

Fig. 6a clearly shows that the cell capacity increases as the Na wetting angle on the BASE decreases; full capacity was obtained for the LAT_400 $^\circ\text{C}$ cell, which has the smallest Na wetting angle among tested cells. A schematic view of a cell with good Na wetting on the BASE surface is shown in Fig. 6b. With good Na wetting, it is possible to utilize the whole area of the BASE (i.e., Na⁺ ion transport occurs evenly over the entire BASE surface) and the cathode materials in LAT_400 $^\circ\text{C}$ can be cycled without any problems. In contrast with the good Na wetting, Fig. 6c shows a cell with extremely poor Na wetting. As shown in Fig. 6c, the Na⁺ ions can only be transported through limited areas where the Na wetting occurs on the BASE surface; thus, only the cathode materials close to the wetting points can be utilized during cell cycling. The majority of the cathode materials cannot be cycled due to a large cell overpotential, which is from the reduced active area (high ohmic resistance) of

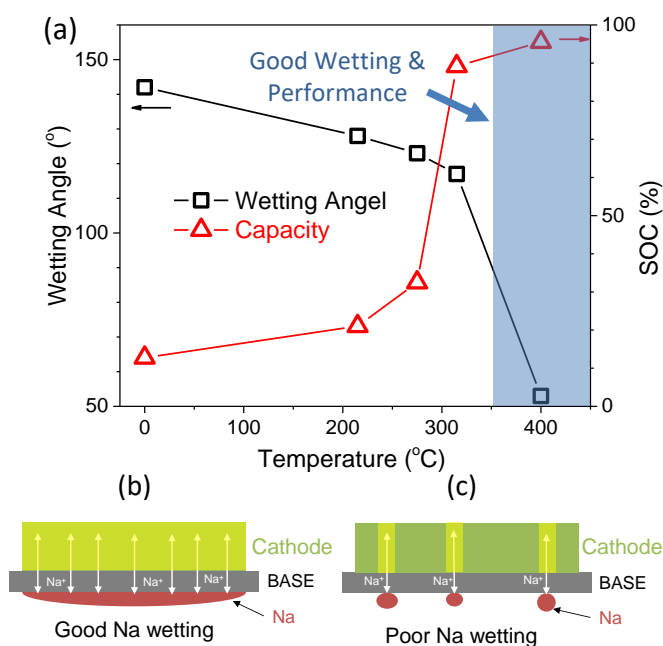


Figure 6. (a) Plots of wetting angle and cell capacity vs. LAT heat-treating temperature. Schematic view of the cathode utilization in the cells with (b) good Na wetting and (c) poor Na wetting.

the BASE and the mass transfer limit (longer distance for Na⁺ transportation in the cathode). The Na wetting in LAT_210°C, LAT_275°, and LAT_315°C cells most likely falls between the two extreme cases shown in Fig. 6b and 6c, respectively, and show degraded capacities that depend on the degree of Na wetting in each cell.

It is worth noting that the sodium wettability has been generally explained using the relation of Young-Dupré on a solid surface, and a more popular equation was later suggested by Adam as following:³⁰⁻³²

$$W_{adh} = \gamma_m \cdot (1 + \cos\theta)$$

where W_{adh} is the work of adhesion between the liquid Na and the BASE, γ_m is the surface tension of the liquid Na, and θ is the wetting angle. For instance, the wettability of a Na/Cs alloy on the BASE surface was examined in our previous study, and the wettability of the Na/Cs alloy on the BASE was drastically improved due to the larger W_{adh} and smaller γ_m of the Na/Cs alloy compared to that of liquid Na.¹⁴

One concern for applying the Young-Dupré relation for Na wetting on LAT_400°C BASE in this work is that the Young-Dupré relation represents the wetting phenomenon on an ideal (smooth) surface.³³⁻³⁶ As one can see from Fig. 3d (SEM), Fig. 3h (Pb mapping), and Fig. S4 (cross-section view), the surface of LAT_400°C BASE is mainly decorated with spherical Pb particles (~1–2 μm) forming a monolayer, which leads us to seek other models to explain the enhanced Na wetting phenomena on Pb-decorated BASE. It has been proposed in the literature that the wetting of a liquid droplet on a rough (jagged) surface typically can be described by three different situations:³⁷ the Cassie model,³⁸ the Wenzel model,³⁹ and the sunny-side-up model,⁴⁰⁻⁴¹ (which resembles an egg fried without being inverted) as shown in Fig. 7. The Cassie model (Fig. 7a) describes an existence of air pocket (N₂ gas here) between the bottom of the liquid drop and the rough surface. Since the liquid drop does not

wet the surface, a larger wetting angle tends to be found for a Cassie drop. In the Wenzel model (Fig. 7c), the liquid at the bottom of the drop penetrates into the texture. The transition from Cassie drop to Wenzel drop could take place by forming a transition state—a Mushroom drop—(Fig. 7b), which has a nucleated patch of liquid that contacts the surface underneath the liquid drop.⁴² The transition to a sunny-side-up drop has been described by in the literature as well. Briefly, under certain conditions such as that the total surface energy decreases as the liquid penetration progresses, a thin liquid film can expand along surface cavities without overflowing the top of the texture on the rough surface.⁴⁰⁻⁴¹ The Na wettings on LAT_400°C shown in Fig. 7 agree quite well with these wetting models. For example, a Na droplet does not wet the surface of LAT_400°C when the surface temperature is 150°C, and the poor wetting is consistent with its large wetting angle (146°, Fig. 7e). That Na droplet could be easily rolled off the surface without leaving any traces of Na wetting mark, which is a characteristic of a Cassie drop. When the temperature was raised to 175°C, the Na wetting on the surface improved and the wetting angle was reduced to 108°, as shown in Fig. 7f. A clear wetting regime (Fig. 7i) was observed after the Na droplet was removed by a glass pipette (the Na droplet was quite sticky), which indicates that the Na liquid penetrates into the Pb texture below the Na droplet. When the temperature reached 200°C, a penetration film quickly developed around the Na droplet, and a sunny-side-up shape was observed (Fig. 7j).

Clearly, the Na wettability on the LAT_400°C is increasing while the surface temperature increases. This temperature dependent Na wetting phenomena intrigued us to think about the possible existence of the surface barrier, which requires an activation energy for Na wetting. We carried out high resolution XPS measurement for LAT-400°C BASEs and observed XPS bands corresponding to Pb 4f_{2/5} (146-141 eV) and Pb 4f_{7/2} (141-136 eV), as shown in Fig. 8 (C1s peaks for Fig. S5). It is surprising to observe an additional band at 138.9 eV (Pb⁰ peak is at 136.8 eV), which matches well with Pb (II) species.⁴³⁻⁴⁴ By considering XPS and XRD spectra, we concluded that Pb particles on LAT-

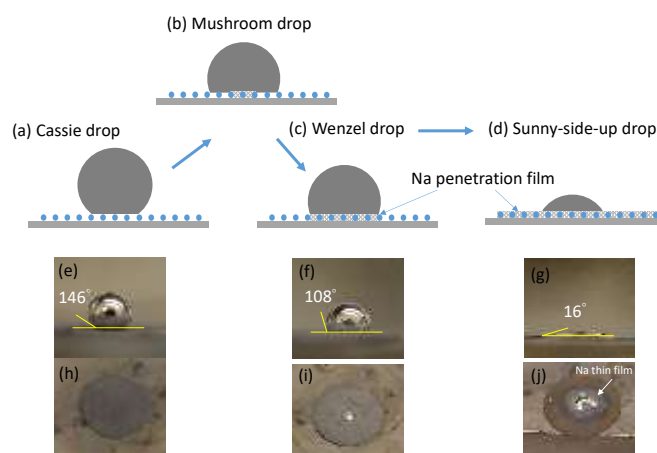


Figure 7. Simplified schematic views of sodium drops on Pb-decorated BASEs. (a) Cassie drop, (b) Mushroom drop, (c) Wenzel drop, and (d) Sunny-side-up drop. Front views of liquid Na sessile drop experiments on LAT_400°C measured at (e) 150°C, (f) 175°C, and (g) 200°C. The corresponding top-view pictures of BASE at (h) 150°C, (i) 175°C, and (j) 200°C.

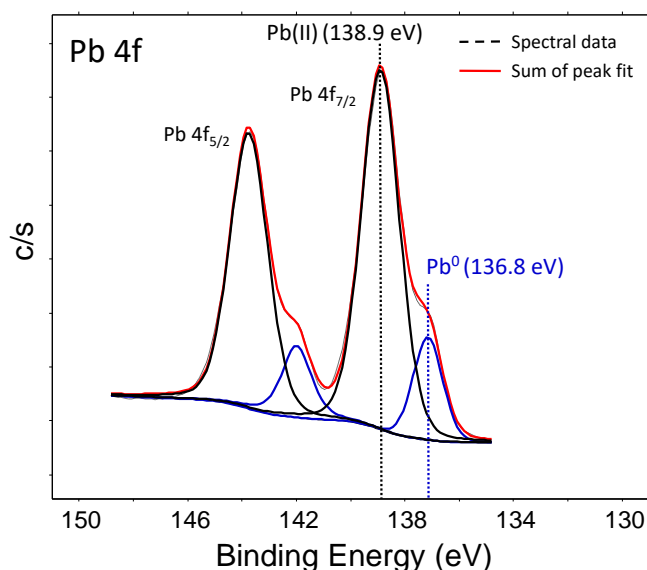


Figure 8. High energy resolution XPS spectrum for LAT-400°C BASE.

400°C BASEs are passivated by a very thin (~5 nm) Pb (II) compounds (PbO or PbCO₃) layers, since it is only observable for XPS spectra (a surface sensitive method) not from XRD (a bulk phase measurement). Indeed, on the basis of high resolution XPS measurements on LAT-400°C BASE, the presence of Pb (II) compounds passivation layers on the surface of Pb micron-particles was clearly identified. It should be noted that the Na wetting could involve the chemical reduction reaction of Pb (II) compounds at the surface. Therefore, we propose that the breaking Pb (II) layers could be the first step toward a good Na wetting and this step is a temperature dependent process, although it is still not clear how this reduction reaction and reaction products (Na₂O or Na₂CO₃, etc.) will affect the Na wetting. Once molten Na and metallic Pb is in the direct physical contact, Na-Pb alloys will be formed according to the Na-Pb bimetallic phase diagram⁴⁵ (shown in Fig. S6). The presence of Na-Pb alloys were also confirmed by ²³Na MAS NMR (Fig. S7) and XRD (Fig. S8) measurements for BASEs retrieved from the LAT-400°C cell at the discharge state, which has least amount of Na on the anode (minimize the signal interference from metallic Na). Similar to the situations of Na-Cs and Na-Bi alloys reported in literatures^{14, 23}, Na-Pb alloy could promote the Na wetting on the LAT-400°C BASE surface.

Finally, we want to discuss how crucial the sunny-side-up shape of Na wetting is for the performance of Na-MH batteries. As it has been described in the experimental section, Na-NiCl₂ batteries tested in this work were typically assembled in the discharged state, which consists of only NaCl and Ni in the cathode. In other words, the batteries do not require preloading of any metallic sodium (the Na will be generated during the charging process), in principle, at the anode as it is assembled. It seems ironic that the battery requires no Na at the beginning although it needs a good Na wetting. Based on the Na wetting in sunny-side-up shape observed for the LAT_400°C BASE, it is most likely that the Na generated during charging quickly makes penetrates and forms a thin film on the LAT_400°C BASE, which

initiates good Na wetting. Our works discovered strategically designed micron-size spherical Pb particles on the BASEs seem to play a critical role in initiating a sunny-side-up Na wetting, which leads to a good battery performance at lower operating temperatures.

Experimental

Wettability test: The sessile drop method was applied to measure the contact angle (θ) of liquid sodium on BASE surfaces in a nitrogen-purged glove box (oxygen and H₂O <0.1 ppm). To study the Na wetting behavior of BASEs, the BASE surface was drop-cast from an aqueous solution of saturated LAT (Pb(CH₃COO)₂•3H₂O >99%, Sigma Aldrich) and heat treated at different temperatures of 210°C, 275°C, 315°C, and 400°C under nitrogen gas atmosphere. Then BASEs were placed on a temperature-controlled hot plate, and a drop of liquid sodium was placed on the BASE. The contact angle was measured at various temperatures from 150°C to 250°C. Pictures of sodium drops were captured 1 min and 30 min after application to the BASE surface to verify that the contact angle was constant. Fig. 1 is a schematic diagram of sessile drops. By definition of wetting of liquid on a solid surface, a smaller contact angle (θ < 90°) implies better wetting.

Cell preparation: Homemade β "-alumina/yttria-stabilized zirconia composite solid-state electrolyte (BASE) discs were fabricated by the vapor phase conversion process as described in previous reports.^{6, 27} The final thickness of the BASE discs is ~500 μ m, with a diameter of 1 inch. BASE discs were glass-sealed to α -alumina fixtures, and the helium leak test was performed to confirm no leakage from the glass-sealed BASE and α -alumina fixture. The surface of BASE facing the anode side was treated with LAT at various designated temperatures. The cathode powder was prepared by low-energy ball-milling a mixture of Ni powder (Novamet, Type 225, particle size <2 μ m), NaCl powder (Alfa Aesar, 99.9%), and additives such as Al, NaI, NaF, and FeS (Sigma Aldrich, >99%) overnight. The molar ratio of Ni to NaCl used in this study was 1.82. After ball-milling, the cathode powder was granulated into ~1 mm size grains using a granulator (Freund TF-LABO). Sodium tetrachloroaluminate (NaAlCl₄), which is called a secondary electrolyte or melt, was prepared through high temperature synthesis by mixing AlCl₃ and a 10% excess of NaCl powder to avoid the formation of Lewis-acidic melts. The cell consisted of cell caps (stainless steel), α -alumina (99.5% purity) fixtures, current collectors (molybdenum foil for the cathode, stainless steel shim for the anode), BASE, and two polymer rings (McMaster-Carr) of fluorinated ethylene propylene (FEP) for cathode and polyvinylidene fluoride (PVDF) for anode to seal the cell components. A total of 1 g of cathode and 0.7 g of melt were loaded on the cathode side and vacuum infiltration was carried out to distribute the melt uniformly throughout the cathode granules at an elevated temperature of 200°C. On the anode side, a small amount of solid sodium was added onto the anode shim to facilitate the initial contact between the BASE and the anode shim. Subsequently, the cells were enclosed with the cell caps and screwed shut to complete the cell assembly. All assembly and disassembly procedures were carried out in a nitrogen-purged glove box (oxygen and H₂O <0.1 ppm). In this study, the cell capacity of 157 mAh (52.3 mAh/cm²) was calculated without considering the mass of the melts.

Battery Cycling Test: Assembled cells were tested in a temperature-controlled furnace in air at 190°C. Galvanostatic tests were carried out using an Arbin potentiostat (MSTAT 8000). Initial cycling (the conditioning process) for the cells was performed between the cutoff voltages of 2.8 V (charge limit) and 1.8 V (discharge limit). The first cycle of the conditioning process consisted of three steps with three different charging currents (0.6 mA for 2 hours, 1 mA for 10 hours, and 10 mA thereafter) and a discharge step at 10 mA. After the first cycle, a current of 10 mA was used for charge/discharge until 10 cycles had been completed. For long-term and regular cycling tests, a charge current of 20 mA (6.7 mA/cm²) and a discharge current of 30 mA (10 mA/cm²) were used.

Thermal Gravimetric Analysis (TGA) /Differential Scanning Calorimetry (DSC): To study the thermal properties of lead acetate, TGA and DSC analyses were conducted. The thermal decomposition of lead acetate powder was measured over a temperature range from 25 to 500°C in the nitrogen atmosphere using a NETZSCH-STA-449C thermal analyzer with a heating rate of 10°C/min.

X-ray Diffraction Spectroscopy (XRD): XRD was carried out to analyze lead acetate and the solid products of heat-treated lead acetate at various temperatures. XRD patterns were obtained using a Rigaku MiniFlex II X-ray diffractometer (Cu K α radiation at $\lambda = 1.5406 \text{ \AA}$, 30 kV, and 15 mA). For sample preparation, lead acetate powders that had been heat treated at different temperatures were collected directly from the BASEs in a nitrogen-purged glove box, and placed on a standard sample holder. Then, the sample holder was sealed with Kapton tape to minimize air exposure during the measurements.

Scanning Electron Microscopy (SEM): The morphological feature of the lead acetate products after heat treatment at various temperatures, the BASE surfaces were carefully analyzed by a JEOL JSM-7100F field emission scanning electron microscope. Energy-dispersive X-ray spectroscopy (EDX) analysis was performed for the element mapping on an Oxford Instruments system.

X-Ray Photoelectron Spectroscopy (XPS): XPS measurement on LAT₄₀₀°C was performed using a Physical Electronics Quantum 2000 Scanning SECA Microprobe, which has a focused monochromatic Al K α X-ray (1486.7 eV) source and a spherical section analyzer. LAT₄₀₀°C sample was prepared in the nitrogen purged glove box and later was transferred to an Ar purged glove box attached to XPS system. Then, the sample was loaded into XPS detection chamber from the Ar purged glove box to avoid any exposure to the air during the sample handling process.

Solid-State Nuclear Magnetic Resonance (NMR) Spectroscopy: ²³Na magic angle spinning (MAS) nuclear magnetic resonance (NMR) experiments were performed on a 600 MHz solid-state NMR spectrometer (Bruker, Germany) with a 3.2 mm HXY probe at a spinning speed of 10 kHz and at room temperature. The 90 degree pulse length and repetition delay were 2 μ s and 3 s, respectively. The Na/Pb samples were scrubbed from the LAT₄₀₀°C and loaded into the NMR rotor (3.2 mm).

Conclusions

We performed extensive material characterizations, Na sessile drop experiments, and battery tests for LAT-treated BASEs at different heat-treatment temperatures to understand the

correlation between the Na wetting and the surface treatment. The texture of LAT heat-treated BASEs shows drastically different morphologies depending on the heat-treating temperature. The Na sessile drop experiments on LAT-treated BASEs indicate that the Na wetting falls under various wetting models such as Cassie drop, Wenzel drop, and sunny-side-up drop depending on the texture of the surface and the temperature. In particular, the Na wetting experiment shows that the Na wetting on LAT₄₀₀°C BASEs is in a sunny-side-up shape (Na penetration film) at 200°C. We concluded that the unique texture consisting of micron-size Pb spherical particles is responsible for creating the Na penetration film (~200°C) on the BASE surface, which leads to superior battery performance. This work demonstrates, for the first time, a strategic approach for improving Na wetting through forming a thin Na penetration film on the BASEs, which is critical for operating Na-MH batteries at a relatively lower temperature (<200°C). Although further studies are required to understand the mechanism of forming sunny-side-up Na wetting, this approach opens a door to improving Na wetting in batteries that use molten Na anodes.

Conflicts of interest

There are no conflicts to declare

Acknowledgements

This work was supported by the U.S. Department of Energy (DOE) Office of Electricity Delivery and Energy Reliability (Contract No. 70247) and the International Collaborative Energy Technology R&D Program of the Korea Institute of Energy Technology Evaluation and Planning funded by the Ministry of Trade, Industry and Energy (No. 20158510050010) and POSCO, the Republic of Korea. XPS measurements was performed using EMSL, a DOE Office of Science User Facility sponsored by the Office of Biological and Environmental Research. Pacific Northwest National Laboratory is a multiprogram national laboratory operated by Battelle Memorial Institute for the DOE under Contract DE-AC05-76RL01830.

Notes and references

1. H. Kim, D. A. Boysen, J. M. Newhouse, B. L. Spatocco, B. Chung, P. J. Burke, D. J. Bradwell, K. Jiang, A. A. Tomaszowska, K. L. Wang, W. F. Wei, L. A. Ortiz, S. A. Barriga, S. M. Poizeau and D. R. Sadoway, *Chem Rev*, 2013, **113**, 2075-2099.
2. Z. G. Yang, J. L. Zhang, M. C. W. Kintner-Meyer, X. C. Lu, D. W. Choi, J. P. Lemmon and J. Liu, *Chem Rev*, 2011, **111**, 3577-3613.
3. B. Dunn, H. Kamath and J. M. Tarascon, *Science*, 2011, **334**, 928-935.
4. S. Ha, J. K. Kim, A. Choi, Y. Kim and K. T. Lee, *Chemphyschem*, 2014, **15**, 1971-1982.
5. N. Yabuuchi, K. Kubota, M. Dahbi and S. Komaba, *Chem Rev*, 2014, **114**, 11636-11682.
6. X. C. Lu, J. P. Lemmon, V. Sprenkle and Z. G. Yang, *Jom-US*, 2010, **62**, 31-36.

7. K. B. Hueso, M. Armand and T. Rojo, *Energ Environ Sci*, 2013, **6**, 734-749.
8. B. Battke, T. S. Schmidt, D. Grosspietsch and V. H. Hoffmann, *Renew Sust Energy Rev*, 2013, **25**, 240-250.
9. K. B. Hueso, V. Palomares, M. Armand and T. Rojo, *Nano Res*, 2017, **10**, 4082-4114.
10. G. S. Li, X. C. Lu, J. Y. Kim, V. V. Viswanathan, K. D. Meinhardt, M. H. Engelhard and V. L. Sprenkle, *Adv Energy Mater*, 2015, **5**, 1500357.
11. G. S. Li, X. C. Lu, J. Y. Kim, K. D. Meinhardt, H. J. Chang, N. L. Canfield and V. L. Sprenkle, *Nat Commun*, 2016, **7**, 10683.
12. X. C. Lu, G. L. Li, J. Y. Kim, J. P. Lemmon, V. Sprenkle and Z. G. Yang, *J Power Sources*, 2012, **215**, 288-295.
13. H. J. Chang, X. C. Lu, J. F. Bonnett, N. L. Canfield, S. Son, Y. C. Park, K. Jung, V. L. Sprenkle and G. S. Li, *J Power Sources*, 2017, **348**, 150-157.
14. M. E. Bowden, K. J. Alvine, J. L. Fulton, J. R. Lemmon, X. Lu, B. J. Webb-Robertson, S. M. Heald, M. Balasubramanian, D. R. Mortensen, G. T. Seidler and N. J. Hess, *J Power Sources*, 2014, **247**, 517-526.
15. C. C. Addison, D. H. Kerridge and J. Lewis, *J Chem Soc*, 1954, DOI: DOI 10.1039/jr9540002861, 2861-2866.
16. F. E. Poindexter and M. Kernaghan, *Phys Rev*, 1929, **33**, 0837-0843.
17. https://en.wikipedia.org/wiki/Surface_tension, Surface Tension).
18. J. L. Sudworth and A. R. Tilley, *The Sodium Sulfur Battery*, Kluwer, New York, 1985.
19. L. Viswanathan and A. V. Virkar, *J Mater Sci*, 1982, **17**, 753-759.
20. J. L. Sudworth, *J Power Sources*, 2001, **100**, 149-163.
21. Y. Y. Hu, Z. Y. Wen, X. W. Wu and J. Jin, *J Power Sources*, 2012, **219**, 1-8.
22. D. Reed, G. Coffey, E. Mast, N. Canfield, J. Mansurov, X. C. Lu and V. Sprenkle, *J Power Sources*, 2013, **227**, 94-100.
23. K. Ahlbrecht, C. Bucharsky, M. Holzapfel, J. Tubke and M. J. Hoffmann, *Ionics*, 2017, **23**, 1319-1327.
24. *UK Pat. 2,067,005 Pat.*, 1982.
25. G. S. Li, X. C. Lu, J. Y. Kim, J. P. Lemmon and V. L. Sprenkle, *J Power Sources*, 2014, **249**, 414-417.
26. G. S. Li, X. C. Lu, J. Y. Kim, J. P. Lemmon and V. L. Sprenkle, *J Mater Chem A*, 2013, **1**, 14935-14942.
27. *U.S. Pat. 6,117,807 Pat.*, 1998.
28. M. A. Mohamed, S. A. Halawy and M. M. Ebrahim, *Thermochim Acta*, 1994, **236**, 249-262.
29. F. J. Martinez-Casado, M. Ramos-Riesco, J. A. Rodriguez-Cheda, F. Cucinotta, E. Matesanz, I. Miletto, E. Gianotti, L. Marchese and Z. Matej, *Inorg Chem*, 2016, **55**, 8576-8586.
30. T. Young, *Phil. Trans. R. Soc. Lond.*, 1805, **95**, 65-87.
31. N. K. Adam, *Nature*, 1957, **180**, 809-810.
32. M. E. Schrader, *Langmuir*, 1995, **11**, 3585-3589.
33. T. S. Chow, *J Phys-Condens Mat*, 1998, **10**, L445-L451.
34. P. S. Swain and R. Lipowsky, *Langmuir*, 1998, **14**, 6772-6780.
35. L. Barbieri, E. Wagner and P. Hoffmann, *Langmuir*, 2007, **23**, 1723-1734.
36. C. W. Extrand, *Langmuir*, 2002, **18**, 7991-7999.
37. C. Ishino, K. Okumura and D. Quere, *Europhys Lett*, 2004, **68**, 419-425.
38. A. B. D. Cassie and S. Baxter, *T Faraday Soc*, 1944, **40**, 0546-0550.
39. R. N. Wenzel, *Ind Eng Chem*, 1936, **28**, 988-994.
40. C. Ishino and K. Okumura, *Eur Phys J E*, 2008, **25**, 415-424.
41. L. Courbin, E. Denieul, E. Dressaire, M. Roper, A. Ajdari and H. A. Stone, *Nat Mater*, 2007, **6**, 661-664.
42. C. Ishino and K. Okumura, *Europhys Lett*, 2006, **76**, 464-470.
43. K. S. Kim, T. J. O'leary and N. Winograd, *Anal Chem*, 1973, **45**, 2214-2218.
44. A. V. Naumkin, A. Karunt-Vass, S. W. Gaarenstroom and C. J. Powell, *Journal*, 2012.
45. A. D. Efanov, N. I. Loginov, A. V. Morozov and A. S. Mikheyev, *J. Phys.: Conf. Ser.*, 2008, **98**, 032013.

Na wetting in sunny-side-up shape is observed on β'' -alumina surface decorated with the micron-size lead spherical particles.

